Bioorganic Chemistry 105 (2020) 104372

Contents lists available at ScienceDirect

Bioorganic Chemistry

journal homepage: www.elsevier.com/locate/bioorg

Coumarin-based fluorescent biosensor with large linear range for ratiometric measurement of intracellular pH

Dalila Iacopini [a], Aldo Moscardini [b], Francesca Lessi [c], Valeria Di Bussolo [a], Sebastiano Di Pietro [d,*], Giovanni Signore [b,c,*]

[a] Dipartimento di Chimica e Chimica Industriale, Università di Pisa, Via G. Moruzzi 3, 56124 Pisa, Italy
[b] NEST, Scuola Normale Superiore and Istituto Nanoscienze-CNR, Piazza San Silvestro, 12, 56127 Pisa, Italy
[c] Fondazione Pisana per la Scienza, via F. Giovannini 13, 56017 San Giuliano Terme (PI), Italy
[d] Dipartimento di Farmacia, Università di Pisa, Via Bonanno 33, 56126 Pisa, Italy

ARTICLE INFO

This article is dedicated to the memory of our friend Alberto Marini.

Keywords:
Fluorescent probes
pH sensing
Ratiometric imaging
Coumarin
Triazines

ABSTRACT

Intracellular pH is a critical parameter involved in cell machinery, and its dysregulation can either cause or signal pathologic states. Currently described fluorescent pH probes are based on single acid-base equilibria, and for this reason are intrinsically unable to capture the wide range of cell pH, usually spanning over more than four units. Here we describe a fluorescent pH biosensor based on a conjugated coumarin-triazine scaffold that is excitable in the visible range, shows pseudo-linear ratiometric response over more than 6 pH units with a single fluorogenic unit, and allows imaging of the whole *endo*-lysosomal pH landscape of living cells with a single acquisition. The probe can discriminate, on the basis of intracellular acidity, between physiologic and tumor cells, being potentially suitable in perspective as diagnostic tool.

1. Introduction

Fluorescent dyes are an established tool to investigate molecular processes at cell and subcellular level. Transient modifications in physical parameters can in fact signal -or cause- pathologic states [1,2] and are increasingly recognized as important hallmark of cell regulation [3]. For this reason, an increasing interest has risen in recent years in the field of environmentally sensitive probes to measure intracellular pH [4–6], dielectric constant [7,8], or viscosity [9]. Despite the important advances in the development of new fluorescent platforms, the availability of fluorescent biosensors excitable a biocompatible wavelengths with large dynamic range is still very limited, especially for the measurement of physico-chemical parameters that rely on the equilibrium between two differently emissive states. A striking example is represented by pH sensitive biosensors, whose detection principle is based on the presence of conjugated base-acid pairs with different emission. The presence of a single protonation site leads to a limited response to pH changes, usually restricted to one pH unit [6]. Such a strict dynamic range represents a particularly severe limitation when a comprehensive insight in complex biologic environments is required. Physiologic cell pH spans from 8 (mitochondria) to 4.5 (lysosomes) in normal conditions, with even more extreme values routinely observed in specific organisms (e.g. acidophilus bacteria) [10–12]. Additionally, subtle pH changes occur -and to a certain extent drive- endocytic vesicle processing [5]. Overall, pH range in living cells simply spans over a range far too wide to allow reliable measurements to be carried out exploiting the linear response range of a single sensor. This is particularly frustrating in view of the increasing interest in the use of pH as a guideline to detect circulating tumour cells [13] and in the study of *endo*-lysosomal environment [3], which is reportedly dysregulated in several pathologies [14]. Notably, pH imbalance, both at intracellular [15] and extracellular [16] level, is a well described tumour hallmark, strictly bound to altered glycolytic metabolism [17] and to a strict interplay between charge-changing mutations in proteins and adaptability to altered pH values [18].

Even in the ideal scenario of a sensor perfectly centered on the pH interval of interest, any variation at the extremes of this scale would be filtered out by the lack of sensitivity of the sensor at the extremes of equilibrium curve. Composite sensors formed by using two or more fluorescent probes with different pK_a can be engineered to address this

* Corresponding authors.
E-mail addresses: sebastiano.dipietro@unipi.it (S. Di Pietro), g.signore@fpscience.it (G. Signore).

https://doi.org/10.1016/j.bioorg.2020.104372
Received 16 July 2020; Received in revised form 11 September 2020; Accepted 8 October 2020
Available online 12 October 2020

issue [19]. Unfortunately, the presence of multiple fluorophores makes challenging their applicability to advanced imaging techniques, that usually require a single emitting unit. Indeed, the presence of two emissive units can easily lead to selective photobleaching that in turns causes poor accuracy in the measurement.

Several scaffolds have been proposed as fluorescent pH sensors [20,21]. Yet, most of them rely on combination of two or more dyes [19,22] are based on simple fluorescence intensity change [23], or show a limited linear dynamic range [24,25]. Overall, the challenge of realizing a ratiometric pH probe based on a single fluorophore with large linear dynamic range is still unmet.

2. Material and methods

2.1. Reagents and instruments

All solvents and chemicals were purchased from Sigma-Aldrich and used without further purification. Silica gel 60 F254 sheets (Merck) were used in analytical thin-layer chromatography (TLC). LC chromatographic separation were performed on a Rf Combiflash preparative purification system. Evaporation was performed in vacuo (rotating evaporator). Sodium sulfate was used as drying agent.

1D and 2D-NMR were recorded with a Bruker Avance III 300 spectrometer, using the indicated deuterated solvents. Chemical shifts are given in parts per million (ppm) (δ relative to residual solvent peak for ^{1}H and ^{13}C).

Purity and MS spectra of synthesized compounds were determined using a Shimadzu Nexera UHPC equipped with a diode array detector and interfaced with an ABSciex API 3200 QTRAP mass spectrometer, using the parameters specified below:

LC conditions: column: Phenomenex Proteo column (4.6x250 mm) Mobile phases: water/TFA 100/0.01 v/v and Acetonitrile/Water/TFA 95/100/0.01 v/v.

MS conditions: Ionization mode: ESI. Curtain gas 10 mL/min; Ion spray voltage: 5500 V; Temperature: not used; Declustering potential: 75 V; Entrance potential: 10 V; Collision energy: 50 eV; Collision energy potential: 43 V.

Retention times (HPLC, t_R) are given in minutes. Compound HPLC purity was evaluated at 254 and 220 nm.

2.2. Synthesis of 2,4-dichloro-6-(2,2-dimethoxyethenyl)-1,3,5-triazine (1)

13.5 g of cyanuric chloride (73 mmol) and 35 g of ketene dimethyl acetal (397 mmol) were suspended in diethyl ether (400 mL). Suspension turned yellow almost immediately. Reaction mixture was refluxed for 6 h and left 48 more hours at room temperature. Diethyl ether was then removed in vacuo. Product **1** was resuspended in cyclohexane and filtered, yielding 15 g (90%) of yellow flakes.

^{1}H NMR (300 MHz, $CDCl_3$), δ (ppm) = 3.77 (s, 3H), 3.95 (s,3H), 7.25 (s, 1H). ^{13}C NMR (75 MHz, $CDCl_3$), δ (ppm) = 44.4, 51.1, 53.1, 167.5, 172.3, 176.4.

2.3. Synthesis of 3a-d

2.3.1. General procedure

In a typical reaction, 0.9 g of 2,4-dichloro-6-(2,2-dimethoxyethenyl)-1,3,5-triazine **1** were dissolved in 50 mL of acetonitrile. 2.1 M equivalents of the appropriate nucleophile and 2 M equivalents of of N,N' diisopropyl ethylamine were added, and the mixture refluxed until complete conversion to trisubstituted product was achieved. Solution was diluted with water (25 mL) and trifluoroacetic acid was immediately added until pH 2 was obtained. Solution was stirred 1 h and volatile solvents were removed in vacuo. Aqueous phase was extracted with ethyl acetate, and the resulting organic phase was dried over sodium sulphate and evaporated to dryness, to afford compound **2**. The crude product was dissolved in anhydrous methanol (ethanol was used for **3d**), 1 equivalent of naphthyl hydroxybenzaldehyde was added, followed by five drops of piperidine. The reaction mixture was refluxed until complete conversion was achieved, monitored by HPLC (usually 12–48 h), then cooled and acidified with TFA. Organic solvent was removed in vacuo leaving the last 1–2 mL, water was added (30 mL), and the product was triturated overnight. Finally, the product was filtered on Buchner funnel.

2.3.2. Characterization of 3a

Yellow solid, yield: 87%

^{1}H NMR (300 MHz, $CDCl_3$), δ (ppm) = 9.60 (s, 1H), 8.40 (d, ^{3}J = 8 Hz, 1H), 8.10 (d, ^{3}J = 9 Hz, 1H), 7.94 (d, ^{3}J = 8 Hz, 1H), 7.75 (t, ^{3}J = 7 Hz, 8 Hz, 1H), 7.61 (t, ^{3}J = 7 Hz, 8 Hz, 1H), 7.52 (d, ^{3}J = 9 Hz, 1H), 4.17 (s, 6H).

^{13}C NMR (75 MHz, $CDCl_3$), δ (ppm) = 172.8, 157.4, 155.6, 136.3, 135.6, 130.3, 129.5, 129.2, 128.9, 126.4, 121.7, 121.4, 116.7, 112.8, 55.5.

MS (ESI+, *m/z*):): 337.2, 336.3 [M+H$^+$], 304.2, 293.3, 279.2, 236.2, 222.4.

2.3.3. Characterization of 3b

Yellow solid, overall yield: 82%

^{1}H NMR (300 MHz, $CDCl_3$), δ (ppm) = 9.27 (s, 1H), 8.32 (d, ^{3}J = 8 Hz, 1H), 7.99 (d, ^{3}J = 9 Hz, 1H), 7.90 (d, ^{3}J = 8 Hz, 1H), 7.70 (t, ^{3}J = 7 Hz, 8 Hz, 1H), 7.56 (t, ^{3}J = 7 Hz, 8 Hz, 1H), 7.46 (d, ^{3}J = 9 Hz, 1H), 3.86 (s, 8H), 1.66–1.62 (m, 12H).

^{13}C NMR (75 MHz, $CDCl_3$), δ (ppm) = 168.3, 164.6, 158.4, 154.6, 140.1, 133.9, 130.2, 129.5, 129.0, 128.3, 126.0, 121.7, 116.8, 113.2, 44.3, 25.8, 25.7, 24.9.

MS (ESI+, *m/z*): 443.3, 442.5 [M+H$^+$].

2.3.4. Characterization of 3c

Yellow solid, overall yield: 78%

^{1}H NMR (300 MHz, DMSO-d_6), δ (ppm) = 9.97 (bs, 2H), 9.46 (s, 1H), 8.54 (d, ^{3}J = 8 Hz, 1H), 8.30 (d, ^{3}J = 9 Hz, 1H), 8.11 (d, ^{3}J = 8 Hz, 1H), 7.87–7.79 (bm, 5H), 7.69–7.63 (m, ^{3}J = 9 Hz, 9 Hz, 2H), 7.36–7.31 (m, ^{3}J = 8 Hz, 8 Hz, 4H), 7.08–7.03 (m, ^{3}J = 7 Hz, 7 Hz, 2H).

^{13}C NMR (75 MHz, DMSO-d_6), δ (ppm) = 169.5, 164.4, 157.8, 154.8, 143.4, 141.3, 139.7, 135.3, 130.4, 129.6, 129.5, 129.3, 128.9, 126.8, 123.2, 122.4, 121.0, 117.0, 112.9.

MS (ESI+, *m/z*): 460.3, 459.7, 458.5 [M+H$^+$], 442.4, 298.3.

2.3.5. Characterization of 3d

Yellow solid, overall yield: 84%

^{1}H NMR (300 MHz, DMSO-d_6), δ (ppm) = 9.31 (s, 1H), 8.44 (d, ^{3}J = 8 Hz, 1H), 8.22 (d, ^{3}J = 9 Hz, 1H), 8.04 (d, ^{3}J = 8 Hz, 1H), 7.78–7.74 (m, ^{3}J = 6 Hz, 7 Hz, 1H), 7.62 (t, ^{3}J = 7 Hz, 8 Hz, 1H), 7.54 (d, ^{3}J = 9 Hz), 4.50 (s, 4H), 4.33 (s, 4H), 4.12 (q, ^{3}J = 3.55 Hz, 8H), 1.22 (t, ^{3}J = 7.18 Hz, 6H), 1.13 (t, ^{3}J = 7.18 Hz, 6H).

^{13}C NMR (75 MHz, DMSO-d_6), δ (ppm) = 170.6, 170.2, 169.7, 165.2, 156.9, 155.0, 135.6, 130.2, 129.5, 129.4, 126.8, 122.5, 122.1, 116.9, 112.7, 112.6, 61.2, 52.3, 14.5.

MS (ESI$^+$, *m/z*): A mixture of ethyl and methyl ester was identified. For each compound, the following spectrum was recorded: tetraethyl: 652.5, 651.4, 650.4 [M+H$^+$]; triethyl-methyl: 638.5, 637.5, 636.5 [M+H$^+$]; diethyl-dimethyl: 623.5, 622.4 [M+H$^+$]; ethyl-trimethyl: 609.5, 608.4 [M+H$^+$]

2.4. Synthesis of 4

Compound **3d** (100 mg) was dissolved in methanol (50 mL). 1 M Triethylammonium bicarbonate solution (10 mL) was added to the methanolic solution and the mixture was stirred at 50 °C until complete saponification was achieved (usually 1 h). Reaction mixture was acidified with TFA, volatile solvents were removed in vacuo, and the

resulting solid was collected by filtration.

2.4.1. Characterization of **4**

Yellow solid, isolated yield: 85%

^{1}H NMR (300 MHz, DMSO-d_6), δ (ppm) = 9.40 (s, 1H), 8.54 (t, ^3J = 8 Hz, 5 Hz, 1H), 8.26 (d, ^3J = 9 Hz, 1H), 8.07 (d, ^3J = 8 Hz, 1H), 7.77 (t, ^3J = 7 Hz, 8 Hz, 1H), 7.66–7.57 (m, 2H), 4.42 (s, 4H), 4.29 (s, 4H).

^{13}C NMR (75 MHz, DMSO-d_6), δ (ppm) = 171.8, 171.4, 165.2, 165.2, 157.1, 155.0, 141.8, 135.4, 130.3, 129.5, 129.3, 126.7, 123.0, 122.9, 116.9, 112.9, 49.8.

MS (ESI+, *m/z*): 538.8 [M+H$^+$], 524.0, 474.8, 442.8, 405.4, 290.0, 257.3.

2.5. Spectroscopic characterization

Typically, 1 mL samples were used in appropriate quartz cuvettes (Hellma, Milan, Italy) all displaying an absorption/excitation optical path of 1 cm. Absorption data were recorded at 25 °C in a JASCO V550 spectrophotometer (JASCO Europe, Cremello, Italy) using 1 nm band-pass, 1 nm step-size and 0.25 s integration time. Fluorescence intensity measurements were carried out with a Cary Eclipse fluorometer (Varian, Palo Alto, CA), using 1 nm band-pass, 1 nm step-size and 0.2 s integration time. Quantum yields were determined according to reported procedures, using quinine sulphate as reference dye. pH titration was performed dissolving the dyes in 20/10 mM citrate/phosphate buffer at pH 7. Solution was then gradually acidified by addition of 1 M hydrochloric acid. For each experimental point pH was measured and spectra were corrected for the dilution factor due the added volume.

Sensitivity to cations was evaluated with the same approach, using a sodium acetate (10 mM) solution buffered at pH 4.5. Increasing amounts of 1 M aqueous solution of NaCl, KCl, $MgSO_4$, or $CaCl_2$ were added to the initial solution up to a final concentration of 200 mM Fluorescence emission was corrected for dilution factor and normalized to that measured for the original solution containing only the probe and the initial buffer.

2.6. Cell viability assay

MCF7 and MCF10 cells (7×10^4) were seeded in triplicate into a 96-well plate and allowed to adhere overnight in a humidified atmosphere of 5% CO_2. Cells were treated with increasing volumes of **4** (stock solution: 50 mM in DMSO) to obtain final concentration of 1.56 μM, 3.125 μM, 6.25 μM, 12.5 μM, and 25 μM. Positive control of cell cytotoxicity was obtained by treating the cells with 20% DMSO. Cells were incubated with WST-1 reagent (Clontech Laboratories, Mountain View, CA) for 1 h at 37 °C and the absorbance was read at 450 nm with the Infinite® 200 PRO NanoQuant plate reader (Tecan) to assess viability. Absorbance values were normalized using the absorbance of untreated and 20% DMSO-treated cells as 100% and 0% viability, respectively.

2.7. Live cell imaging and intracellular pH measurement

2.7.1. pH calibration

Compound **4** was dissolved in citrate-phosphate buffer at different pH (3.7, 4, 5.56, 7) at a final concentration of 5 uM. Images were recorded at an excitation wavelength of 405 nm. Channel 1 and channel 2 were set at 415–470 nm and 480–580 nm, respectively. Average intensity for each channel was background subtracted and GP, defined as (Ch1-Ch2)/(Ch1 + Ch2) was plotted against pH. Linear fitting afforded the calibration curve for pH measurement.

2.7.2. Cell culture

MCF7 and MCF10a cells were provided from the American Type Culture Collection (ATCC). MCF7 were grown in low glucose DMEM medium (Thermo Fisher Scientific, Waltham, MA, USA) supplemented with 10% FBS (Thermo Fisher Scientific), 100 U/ml penicillin (Thermo Fisher Scientific) and 100 μg/ml streptomycin (Thermo Fisher Scientific). MCF10a (ATCC CRL10317) were grown in MEGM Mammary Epithelial Cell Growth Medium BulletKit (Lonza, Basel, Switzerland) supplemented with 100 U/ml penicillin (Thermo Fisher Scientific) and 100 μg/ml streptomycin (Thermo Fisher Scientific). Cells were maintained at 37 °C in a humidified 5% CO_2 atmosphere. Cells were incubated for 24 h before imaging. For live imaging, 150.000 cells were plated onto 35-mm glass bottom dish (WillCo-dish GWSt-3522) 24 h prior to experiments at 60–80% confluence. For the experiments, the cells were loaded for 15–30 min with compound **4** (5–10 μM). The fluorescent probe, solubilized in DMSO (25 mM), was dissolved directly in serum-free cell medium.

2.7.3. Imaging in living cells

Cell fluorescence was measured using an Olympus FV3000 inverted confocal microscope interfaced with 405, 488, 561, and 633 nm laser lines. Glass bottom Petri dishes containing cells were mounted in a thermostated chamber at 37 °C and 5% CO_2 and viewed with an UPLSAPO 60x 1.42 NA oil immersion objective. The pinhole aperture was set to 1.0 Airy. Images were collected monitoring the emission using two detection channels (Ch1 and Ch2) set at 415–470 nm and 480–580 nm, respectively. During the experiments, untreated cells were imaged in parallel with the samples to evaluate the potential contribution of cell autofluorescence, whose intensity was maintained below 3% of the fluorophore signal. Data were analysed by Imagej 1.52a package and by Origin-Pro7 package. Image processing involved thresholding of both channels based on their respective background signal (average + 3 s.d.). pH channel was calculated from the thresholded channels using the formula GP= (Ch1-Ch2)/(Ch1 + Ch2). The obtained GP was transformed in pH units using a linear calibration obtained with free fluorophore in buffered solutions.

2.7.4. Imaging of cells buffered at different pH

Imaging of cells buffered at different pH was performed using a commercial Intracellular pH Calibration Buffer Kit (Life Technologies, P35379). Cells were treated according to manufacturer instructions, and after addition of the probe in DMSO images were taken with the same setup describe above. To ensure that no cytotoxic effect from pH alteration occurred, each calibration point was obtained using fresh cells and imaging for each point lasted not more than 30 min.

2.7.5. Colocalization analysis

The subcellular localization of **4** was investigated with fluorescent organelle markers purchased from Invitrogen. All staining protocols (i.e. incubation time/temperature, and medium replacement) were carried out according to the manufacturer's instructions. Lysosomes were selectively stained with Lysotracker Deep Red (10 nM); images were taken by setting λ_{exc} = 640 nm and λ_{em} = 650–700 nm. Mitochondria were stained using Mitotracker deep red, according to the manufacturer instructions. Colocalization analysis and determination of Manders' coefficients were performed by means of the Colocalization Finder plugin of ImageJ image software

3. Results and discussion

In the framework of our long-standing research line on fluorescent biosensors [7,8], we addressed this issue by developing a biosensor with an extended linear response to pH changes. To this end, we focused on coumarin backbone, which is characterized by excellent photophysical properties [7]. To confer pH dependence we selected s-triazine platform as a flexible scaffold to insert pH sensitive units. The use of heteroaromatic substituents to confer pH sensitive properties to coumarin fluorophores has already been reported and leads to good sensitivity in extreme pH conditions [10]. 1,3,5-triazines have been widely investigated as fluorescent whitening agents and as scaffold for dye synthesis [26], and are synthetically attractive due to their easy derivatization by

simple substitution starting from cyanuric chloride. Surprisingly, triazine-substituted coumarins have been almost completely neglected since their first synthesis in 1967 [27,28], and their photophysic behavior is completely unknown. The interesting chemical and photophysical features of triazine-based systems, however, make this platform highly promising to develop solvatochromic fluorescent sensors. To this end, we set up a general synthetic approach reported in Scheme 1, with the aim of obtaining a robust and flexible approach suitable for the development of a palette of triazino coumarin derivatives.

We took advantage of the well-known smooth reactivity of hydroxybenzaldehydes with β-aryl esters in Knoevenagel conditions. We synthesized the necessary triazine ester by simple reaction between ketene dimethyl acetal and trichlorotriazine [29], followed by substitution of the two remaining chlorine atoms with oxygen- or nitrogen-based nucleophiles (Scheme 1). Note that in this work two identical substituents were used, but due to the modulable reactivity of chlorotriazines it is possible to insert two different substituents without increasing synthetic complexity. Work up in aqueous acid conditions afforded the desired intermediates **2a-d** in nearly quantitative overall yields. Condensation with naphthyl hydroxybenzaldehyde lead to the formation of target compounds **3a-d** in excellent yields (Table 1). Starting from tetraester **3d**, we finally obtained the tetraacid **4** by simple saponification in basic aqueous conditions. Notably, all the obtained compounds were purified by simple precipitation from the reaction mixture, without any use of chromatographic separation.

Main photophysical properties of the synthesized dyes are reported in Table 1 and in Table S1. Interestingly, all compounds show absorption maxima at wavelengths typical of coumarin-based systems (370–400 nm), with limited dependence on the nature of substituents on triazine ring. Conversely, fluorescence emission is strongly affected by the nature of substituents: both piperidine- and aniline- substituted derivatives (**3b** and **3c**) show negligible fluorescence emission, while methoxy- and iminodiacetate- substituted **3a**, **3d**, and **4** are emissive at pH 7. Likely, rotational deactivation occurring in nitrogen-substituted triazines leads to the observed loss of fluorescence emission. This deactivation pathway is at least partially inhibited by the more stringent steric requirements in the case of **3d** and **4**. We then examined fluorescence dependence on pH of the synthesized compounds. Amino-substituted derivatives **3b** and **3c** are not emissive at any pH, while compounds **3a** and **3d** show a similar

Table 1
Photophysical characterization of triazinyl coumarins.

	RH	λ_{max} H_2O[a]	λ_{max} DMSO Abs ($\varepsilon \times 10^4$)	λ_{max} (em)[a]	η_{fl} (390 nm)[a]
3a	MeOH	378	378 (1.4)	465	0.61
3b	Piperidine	378	370 (1.2)	n.d.	n.d.
3c	Aniline	386	370 (1.8)	n.d.	n.d.
3d	Diethyl imino-diacetate	387	378 (1.5)	469	0.51[b]
4	Imino-diacetic acid	373	377 (2.8)	460	0.08[c]

[a] Measured at pH = 7.
[b] isolated as a mixture of methyl- and ethyl-esters. Yield calculated on the recovered product and chromatographic area ratio between the esters.
[c] Measured at pH = 4. Fluorescence quantum yield is dependent on pH (Table S1).

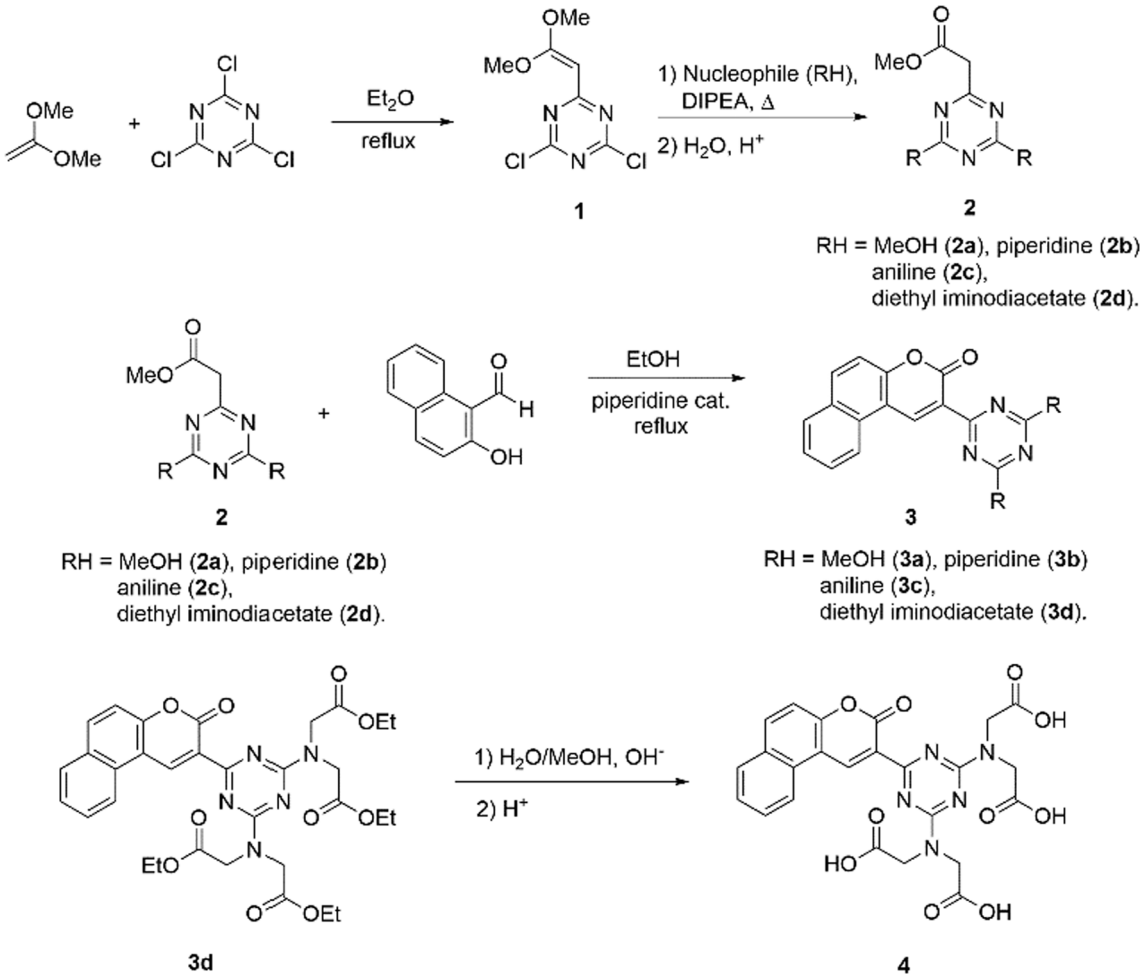

Scheme 1. General synthetic pathway to triazinyl coumarins.

trend involving almost no change in absorption spectrum and 30 nm) emission red-shift in the 1–7 pH interval. Fluorescence emission is almost unaffected in the pH range 3–7 and decreases significantly below this value (Fig. S1). This behavior suggests a marginal role of the nature of the heteroatom substituent on triazine (oxygen or nitrogen) on emission properties, and a limited influence exerted by protonation of nitrogen atoms on the triazine system, that could play a more pronounced role at low pH, as suggested by the bathochromic shift occurring in absorption spectrum (Fig. 1), in agreement with what previously observed for similar systems [10].

Photophysical behavior of tetra acid derivative **4** is more complex and informative. First, absorption spectrum is strongly dependent on pH, with a significant bathochromic shift upon acidification (40 nm between pH 7 and 1, Fig. S1). Emission spectrum is also strongly dependent on pH and red-shifted fluorescence emission is observed at lower pH (Fig. 1a). Of note, fluorescence quantum yield increases at lower pH (Table S1), in contrast with what observed for its analogues **3a,d**. A 35 nm red-shift of fluorescence emission maximum is observed between pH 1 and 7 (Fig. 1a and S2). Note that probe emission is very dim at neutral and basic pH, due to the low fluorescence quantum yields. The observed modulation of fluorescence emission allows selecting appropriate channels for ratiometric emission-based measurement. Based on the observed response, 470 nm was chosen as the most appropriate wavelength to separate the two channels for ratiometric measurements. In these conditions, response of **3a** and **3d** is well

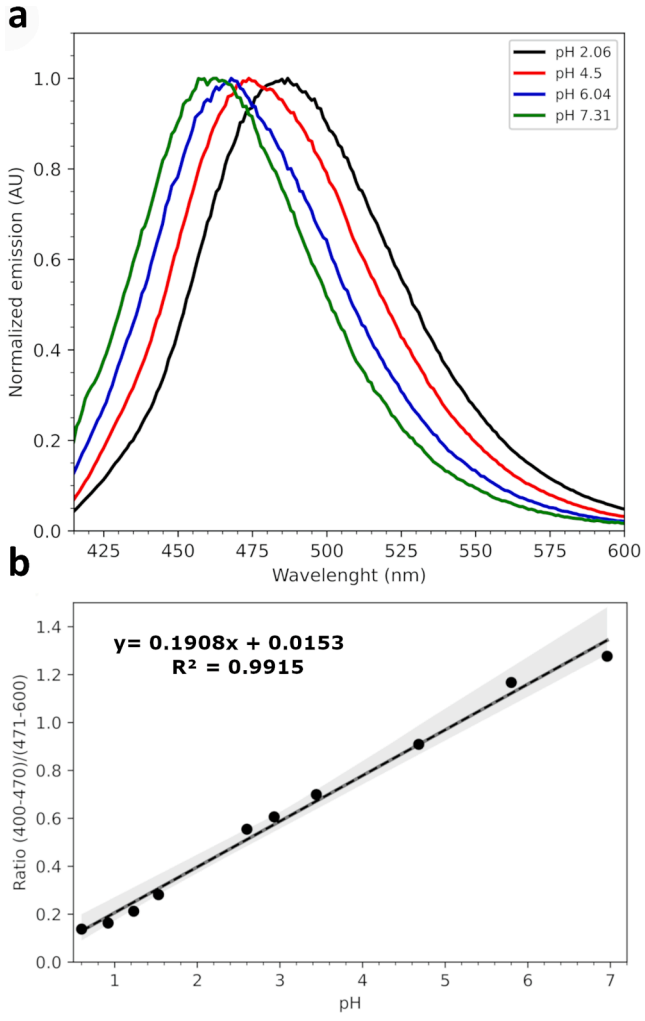

Fig. 1. (a) Normalized fluorescence emission spectra of **4** at different pH; (b) plot of emission ratio (400–470 nm and 471–600 nm) dependence on pH. Confidence interval (99%) is represented as a light grey area.

described by a steep curve centered around pH 2 (Fig. S3) in keeping with the presence of protonable groups at highly acidic pH. Conversely, compound **4** presents an extremely smooth, nearly linear response that extends over six pH units (Fig. 1b, S3).

The observed pH sensitivity is particularly striking if compared with the nearly complete absence of pH response of the tetraester analogue **3d** and suggests that the nitrogen atoms do not play a critical role in modulating pH response at mildly acidic pH. The carboxylic acids are not conjugated to the fluorophore system, thus the most reasonable explanation for the observed pH dependence is the modulation of rotational deactivation of the nitrogen atom with increase in fluorescence quantum yield. The presence of four carboxylic acids leads to the establishment of a series of chemical equilibria between several protonated species, ultimately leading to the observed smooth, seemingly linear pH shift of fluorescence emission not commonly found in two-state ratiometric probes. To further confirm this hypothesis, we performed a preliminary NMR investigation tailored to provide some hints on the sensing mechanism. NMR spectra were recorded at three different pH (6, 4, and 2), and proton chemical shift was compared (Fig. S4). We observed as expected a shift towards high fields, which is, however, dependent on the nature of the proton examined. Indeed, aliphatic protons undergo a more pronounced shift (0.01 ppm) between pH 6 and pH 4 and are less affected (0.005 ppm) by further acidification to pH 2. Aromatic proton in position 4 on the coumarin ring is significantly more affected, and with opposite magnitude. The pH 6 to pH 4 acidification leads to increase of 0.01 ppm, while further acidification to pH 2 has a more important effect (0.04 ppm). Overall, these results seem to indicate that the response of the probe to mildly acidic conditions is largely due to protonation equilibria on the carboxyl groups, while at more acidic pH protonation of nitrogen atoms plays a prominent role. Conversely, **4** is not sensitive to the presence of biologically relevant mono- and divalent cations (Na^+, K^+, Ca^{2+}, Mg^{2+}) up to 200 mM, as shown by the negligible change in fluorescence emission at different ion concentrations (Fig. S5).

Next, we determined whether the observed pH sensitivity in cuvette could be exploited in vitro. To this end, we selected two matched cell lines, MCF7 and MCF10. The former is a metastatic breast cancer cell line, while the latter is an epithelial, non-tumorigenic line which was selected as control. Preliminary experiments demonstrated that the probe is not cytotoxic at least up to 25 μM (Fig. S6). When **4** is administered to cultured cells, diffuse fluorescence is observed, with complete staining of *endo*-lysosomal compartment (Fig. 2) including complete staining of lysosomes (Manders' coefficient: 0.94, Fig. 2a), and to a lesser extent at mitochondria level (Manders' coefficient: 0.71, Fig. 2b). Time-lapse experiments performed with continuous irradiation on the same field evidenced that the probe is photostable in standard imaging conditions (Fig. S7). Finally, we evaluated pH sensing performances of the probe in vitro by measuring the intensity ratio between two emission channels (λ_{exc} 405 nm, λ_{em} 415–470 nm and 480–580 nm for channel 1 and channel 2, respectively). Imaging of MCF7 cells buffered at different pH demonstrates that linear response of the probe observed in cuvette is fully retained in vitro (Fig. S8), thus allowing reliable pH measurement in living cells.

Finally, we set up a comparison between intracellular pH of pathologic and physiologic cells. As expected based on cell physiology, a significant pH overlap was found between physiologic and tumor cells, especially in the 5.5–6.5 region typical of the endosomal pathway. However, when examining the whole pH landscape, it is evident that pH distribution is markedly different between the two cell lines (6.02 and 6.7 for MCF7 and MCF10, respectively. Fig. 3, n = 40 for each cell type). This difference is reflected also in the different distribution of measured pH, which is considerably shifted towards more acidic values in MCF7 compared with their physiologic counterparts. Interestingly, the increased brightness of the probe at acidic pH allows highlighting most cell organelles. As a result, the average pH value reflects staining of the entire *endo*-lysosomal pathway, in agreement with similar

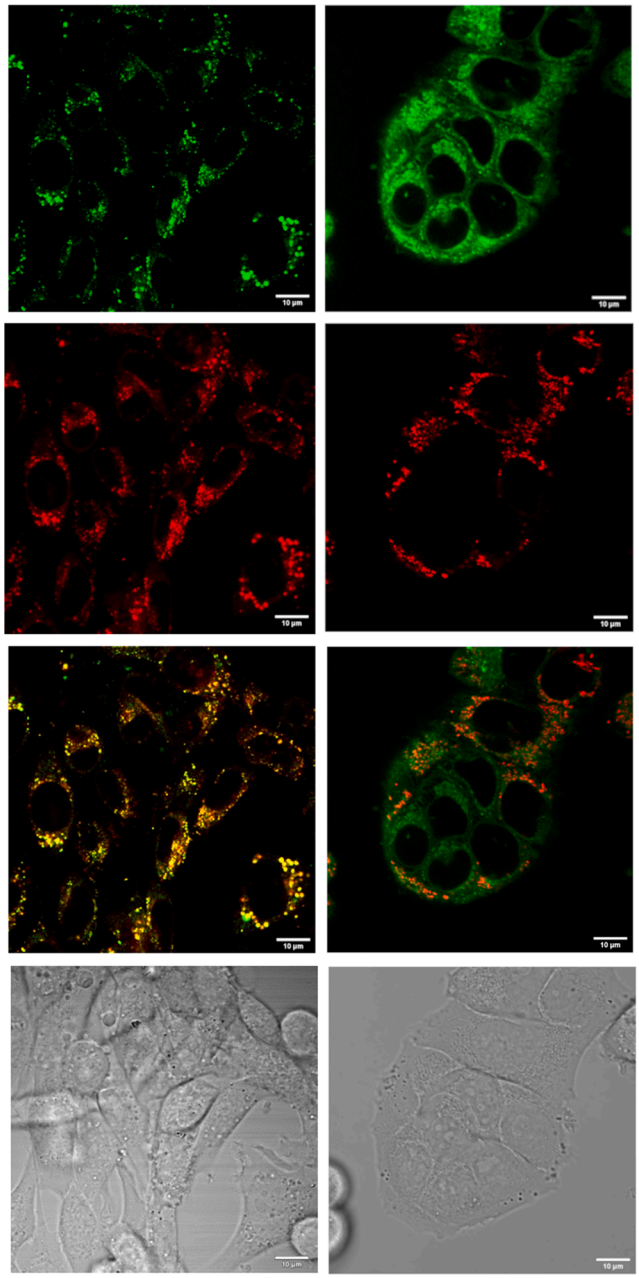

Fig. 2. Colocalization of 4 with lysotracker (left) and mitotracker (right). Probe fluorescence is shown in green, marker fluorescence in red. (For interpretation of the references to colour in this figure legend, the reader is referred to the web version of this article.)

measurements performed with different fluorescent probes [21]. Note, however, that in this study we could capture at once the entire pH pattern of the *endo*-lysosomal system, thus exploiting at its best the large dynamic range of our probe.

The significant difference in sensed pH between physiologic and tumor cells highlights the possibility to distinguish and localize tumor cells even in the presence of physiologic tissues, allowing in perspective precise identification of tumor states at single cell level.

4. Conclusions

In summary, we obtained a universal fluorescent pH sensor based on triazine-derivatized coumarins that provides linear ratiometric response to pH changes spanning six pH units, a three-fold improvement

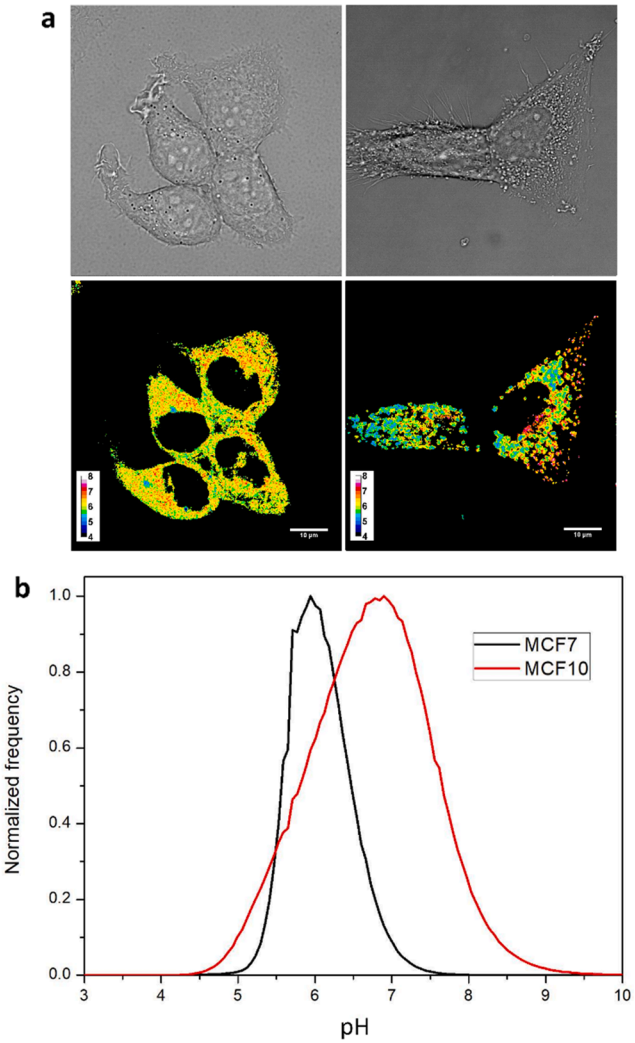

Fig. 3. (a) pH sensing in MCF7 (left) and MCF10a (right) living cells obtained by ratiometric measurement of fluorescence emission from **4** (n = 40 for each case); (b) normalized frequency distribution of pH measured in living cells.

compared with any other single fluorophore reported so far. This impressive range allows achieving a whole picture of endolysosomal pathway at once, thus giving a more comprehensive vision of intracellular pH variations. The possibility to maintain strict linearity up to exceptionally low pH could allow monitoring even the most extreme variations and fluctuations in intracellular pH and find potential applications in life science, material science, and microscopy. Finally, the high modularity conferred by the presence of the conjugated triazine ring paves the way to the development of highly specific biosensors for single- or dual-sensing applications or to improve fluorescence properties. Further studies are in progress to evolve this platform in more optically performing systems by rational design.

Funding

This research did not receive any specific grant from funding agencies in the public, commercial, or not-for-profit sectors.

Declaration of Competing Interest

The authors declare that they have no known competing financial interests or personal relationships that could have appeared to influence the work reported in this paper.

Appendix A. Supplementary material

Supplementary data to this article can be found online at https://doi.org/10.1016/j.bioorg.2020.104372.

References

[1] H. Izumi, T. Torigoe, H. Ishiguchi, H. Uramoto, Y. Yoshida, M. Tanabe, T. Ise, T. Murakami, T. Yoshida, M. Nomoto, K. Kohno, Cellular pH regulators: potentially promising molecular targets for cancer chemotherapy, Cancer Treatment Rev. 29 (6) (2003) 541–549.

[2] L.E. Gerweck, K. Seetharaman, Cellular pH gradient in tumor versus normal tissue: potential exploitation for the treatment of cancer, Cancer Res. 56 (1996) 1194–1198.

[3] F. Begarani, F. D'Autilia, G. Signore, A. Del Grosso, M. Cecchini, E. Gratton, F. Beltram, F. Cardarelli, Capturing metabolism-dependent solvent dynamics in the lumen of a trafficking lysosome, ACS Nano (2019) acsnano.8b07682. https://doi.org/10.1021/acsnano.8b07682.

[4] K.-I. Hong, S.-H. Park, S.M. Lee, I. Shin, W.-D. Jang, A pH-sensitive excited state intramolecular proton transfer fluorescent probe for imaging mitochondria and Helicobacter pylori, Sensors Actuat. B: Chem. 286 (2019) 148–153.

[5] M. Martineau, A. Somasundaram, J.B. Grimm, T.D. Gruber, D. Choquet, J. W. Taraska, L.D. Lavis, D. Perrais, Semisynthetic fluorescent pH sensors for imaging exocytosis and endocytosis, Nat. Commun. 8 (2017) 1–10, https://doi.org/10.1038/s41467-017-01752-5.

[6] P. Cui, X. Jiang, J. Sun, Q. Zhang, F. Gao, A water-soluble rhodamine B-derived fluorescent probe for pH monitoring and imaging in acidic regions, Methods Appl. Fluoresc. 5 (2017) https://doi.org/10.1088/2050-6120/aa69c7.

[7] G. Signore, R. Nifosì, L. Albertazzi, B. Storti, R. Bizzarri, Polarity-sensitive coumarins tailored to live cell imaging, J. Am. Chem. Soc. 132 (4) (2010) 1276–1288.

[8] G. Signore, G. Abbandonato, B. Storti, M. Stöckl, V. Subramaniam, R. Bizzarri, Imaging the static dielectric constant in vitro and in living cells by a bioconjugable GFP chromophore analog, Chem. Commun. 49 (17) (2013) 1723, https://doi.org/10.1039/c3cc38071h.

[9] M.K. Kuimova, G. Yahioglu, J.A. Levitt, K. Suhling, Molecular rotor measures viscosity of live cells via fluorescence lifetime imaging, J. Am. Chem. Soc. 130 (21) (2008) 6672–6673.

[10] Y. Xu, Z. Jiang, Y. Xiao, F.Z. Bi, J.Y. Miao, B.X. Zhao, A new fluorescent pH probe for extremely acidic conditions, Anal. Chim. Acta 820 (2014) 146–151, https://doi.org/10.1016/j.aca.2014.02.029.

[11] S. Wan, Y. Zheng, J. Shen, W. Yang, M. Yin, "On–off–on" switchable sensor: a fluorescent spiropyran responds to extreme pH conditions and its bioimaging applications, ACS Appl. Mater. Interfaces 6 (22) (2014) 19515–19519.

[12] W. Niu, L.i. Fan, M. Nan, Z. Li, D. Lu, M.S. Wong, S. Shuang, C. Dong, Ratiometric emission fluorescent pH probe for imaging of living cells in extreme acidity, Anal. Chem. 87 (5) (2015) 2788–2793.

[13] F. DelBen, M. Turetta, G. Celetti, A. Piruska, M. Bulfoni, D. Cesselli, W.T.S. Huck, G. Scoles, A method for detecting circulating tumor cells based on the measurement of single-cell metabolism in droplet-based microfluidics, Angew. Chem. Int. Ed. 55 (30) (2016) 8581–8584.

[14] A.R.A. Marques, P. Saftig, Lysosomal storage disorders – challenges, concepts and avenues for therapy: beyond rare diseases, J. Cell Sci. 132 (2) (2019) jcs221739, https://doi.org/10.1242/jcs.221739.

[15] D.E. Korenchan, R.R. Flavell, Spatiotemporal pH heterogeneity as a promoter of cancer progression and therapeutic resistance, Cancers (Basel) 11 (2019), https://doi.org/10.3390/cancers11071026.

[16] P. Swietach, What is pH regulation, and why do cancer cells need it? Cancer Metastasis Rev. 38 (1-2) (2019) 5–15.

[17] E. Persi, M. Duran-Frigola, M. Damaghi, W.R. Roush, P. Aloy, J.L. Cleveland, R. J. Gillies, E. Ruppin, Systems analysis of intracellular pH vulnerabilities for cancer therapy, Nat. Commun. 9 (1) (2018), https://doi.org/10.1038/s41467-018-05261-x.

[18] K.A. White, K. Kisor, D.L. Barber, Intracellular pH dynamics and charge-changing somatic mutations in cancer, Cancer Metastasis Rev. 38 (1-2) (2019) 17–24.

[19] J. Qi, D. Liu, X. Liu, S. Guan, F. Shi, H. Chang, H. He, G. Yang, Fluorescent pH sensors for broad-range pH measurement based on a single fluorophore, Anal. Chem. 87 (12) (2015) 5897–5904.

[20] J.-T. Hou, W.X. Ren, K. Li, J. Seo, A. Sharma, X.-Q. Yu, J.S. Kim, Fluorescent bioimaging of pH: from design to applications, Chem. Soc. Rev. 46 (8) (2017) 2076–2090.

[21] S. Takahashi, Y.u. Kagami, K. Hanaoka, T. Terai, T. Komatsu, T. Ueno, M. Uchiyama, I. Koyama-Honda, N. Mizushima, T. Taguchi, H. Arai, T. Nagano, Y. Urano, Development of a series of practical fluorescent chemical tools to measure pH values in living samples, J. Am. Chem. Soc. 140 (18) (2018) 5925–5933.

[22] L. Cao, Z. Zhao, T. Zhang, X. Guo, S. Wang, S. Li, Y.i. Li, G. Yang, In vivo observation of the pH alternation in mitochondria for various external stimuli, Chem. Commun. 51 (97) (2015) 17324–17327.

[23] Z. Li, C. Yu, Y. Chen, Z. Zhuang, B. Tian, C. Liu, P. Jia, H. Zhu, W. Sheng, B. Zhu, A novel water-soluble fluorescent probe with ultra-sensitivity over a wider pH range and its application for differentiating cancer cells from normal cells, Analyst 144 (23) (2019) 6975–6980.

[24] Z. Liu, G. Li, Y. Wang, J. Li, Y. Mi, D. Zou, T. Li, Y. Wu, Quinoline-based ratiometric fluorescent probe for detection of physiological pH changes in aqueous solution and living cells, Talanta 192 (2019) 6–13.

[25] S. Zhu, W. Lin, L. Yuan, Development of a ratiometric fluorescent pH probe for cell imaging based on a coumarin–quinoline platform, Dyes Pigm. 99 (2) (2013) 465–471.

[26] L.i. Liu, Z. Zhou, J. Shi, Z. Liu, C. Lu, W. He, J. Ma, Y. Cui, G.-Y. Lu, Photophysical and two-photon absorption properties of protonation-induced tribranched chromophore having 1,3,5-triazine core and pyrrole end-groups, Synthetic Metals 161 (9-10) (2011) 783–788.

[27] H. Eilingsfeld, H. Scheuermann, Synthese von 1.3.5-Triazinen, Chem. Ber. 100 (6) (1967) 1874–1891.

[28] A. Makowska, F. Saczewski, P.J. Bednarski, J. Saczewski, Ł. Balewski, Hybrid molecules composed of 2,4-diamino-1,3,5-triazines and 2-imino-coumarins and coumarins. Synthesis and cytotoxic properties, Molecules 23 (2018) 1–16, https://doi.org/10.3390/molecules23071616.

[29] E. Kober, The reaction of ketene diethyl acetal with cyanuric chloride, J. Org. Chem. 26 (1961) 4705.